High-energy Neutral Pion Photoproduction

F. Butaru,[1] K. Egiyan,[2] R. Gilman (spokesperson),[3,4] C. Glashausser,[3] O. Hansen,[4] X. Jiang,[3] M. Jones,[4] E. Kuchina,[3] G. Kumbartzki,[3] V. Mamyan,[2] P. Markowitz,[5] Z.-E. Meziani,[1] R. Michaels,[4] S. Nanda,[4] A. Nathan,[6] R. Ransome,[3] B. Reitz,[4] A. Saha,[4] B. Sawatzky,[1] E. Schulte,[3] P. Solvignon,[1] B. Wojtsekhowski (spokesperson),[4] and H. Yao[1]

[1] *Temple University, Philadelphia, Pennsylvania 19122, USA*
[2] *Yerevan Physics Institute, Yerevan, Armenia*
[3] *Rutgers, The State University of New Jersey, Piscataway, New Jersey 08854, USA*
[4] *Thomas Jefferson National Accelerator Facility, Newport News, Virginia 23606, USA*
[5] *Florida International University, Miami, Florida, USA*
[6] *University of Illinois, Urbana, IL 61801, USA*

(Dated: June 28, 2005)

The study of the tomographic structure of the nucleon through generalized parton distributions and the handbag mechanism is a central part of the Jefferson Lab research program. It is widely recognized that the formalism applies to, and needs to be studied with, exclusive meson production reactions in addition to Compton scattering. We propose to measure spin observables in neutral pion photoproduction at high energies, $E_\gamma \approx 5$ GeV, and high momentum transfers, $-t$ of a several GeV^2, with a primary goal of testing recent predictions that use generalized parton distributions, and determining if the handbag mechanism accounts for the data. If this is the case, the measurements provide an insight into the large W, large $-t$ structure of the nucleon, by allowing extraction of generalized form factors. The proposed measurements also provide a point of comparison for the simple spin dynamics observed in $K^+\Lambda^0$ photo- and electro-production, and give constraints on the importance of resonances at high invariant mass. This Hall A experiment builds on the experience developed in previous Hall A photo-polarization measurements.

The experimental technique is the same as that used in a previous Hall A neutral pion photoproduction experiment, except for the addition of a photon calorimeter, as was done in the Hall A RCS experiment. We plan to use the BIGCAL calorimeter being constructed by Halls A and C. The total beam time needed is 22 days.

MOTIVATION

There is a long record of pion photoproduction studies. Near threshold, the reaction is interesting for studies of effective field theories / chiral perturbation theory. At energies of several hundreds of MeV, the reaction is a leading source of information on the properties of baryon resonances. But as energies increase into the multi-GeV range, the pion photoproduction reaction is little understood. Many suggested descriptions of the underlying physics have been proposed, including perturbative quantum chromodynamics (pQCD), pQCD plus an interfering non-perturbative amplitude, generalized parton distributions (GPDs), Regge theory, some times with an approach to pQCD, and hadronic theory.

The idea that is the focus of our interest in this proposal is that pion photoproduction results from the handbag mechanism and can be described with GPDs, starting at energies of about 5 GeV. A confirmation of this would allow a study of the structure of the nucleon at large values of W and $-t$, due to the large photoproduction cross sections. To date, pseudoscaler meson photo-production at energies of a few GeV has proven to be a difficult problem, with no obvious simple underlying physics, as we discuss in the following sections. Furthermore, the behaviours observed in pion photo-production are in sharp contrast to those observed in $K^+\Lambda^0$ photo-production. In the following sections, we first discuss the existing data. We then turn to discussion of calculations of pion photo-production using the handbag mechanism and GPDs. We also, much more briefly, discuss other theoretical ideas, to show what might be learned from a new measurement of high energy and momentum transfer pion photo-production.

Existing pion photoproduction data

There is a variety of older pion photoproduction data at high energies, including:

- cross sections, though only a few angular distributions at high energies and large scattering angles,
- single polarization observables, mostly around 1 GeV, and also
- a limited number of single polarization observables at several GeV, though only at small angles, generally corresponding to Mandelstam $-t < 1$ GeV.

Our first Hall A pion photoproduction experiment [1], E94-012, measured recoil polarizations for $\gamma p \to \pi^0 p$ for large scattering angles and for photon energies up to 4 GeV. The observables included:

$\mathbf{C_{x'}}$: (also called K_{LS}) the transferred polarization component in the reaction plane, perpendicular to the outgoing c.m. momentum,

$\mathbf{p_y}$: the induced polarization component, perpendicular to the reaction plane, and

$\mathbf{C_{z'}}$: (also called K_{LL}) the transferred polarization component in the reaction plane, parallel to the outgoing c.m. momentum.

These are the first data for the polarization transfer observables ever measured (in meson photoproduction).

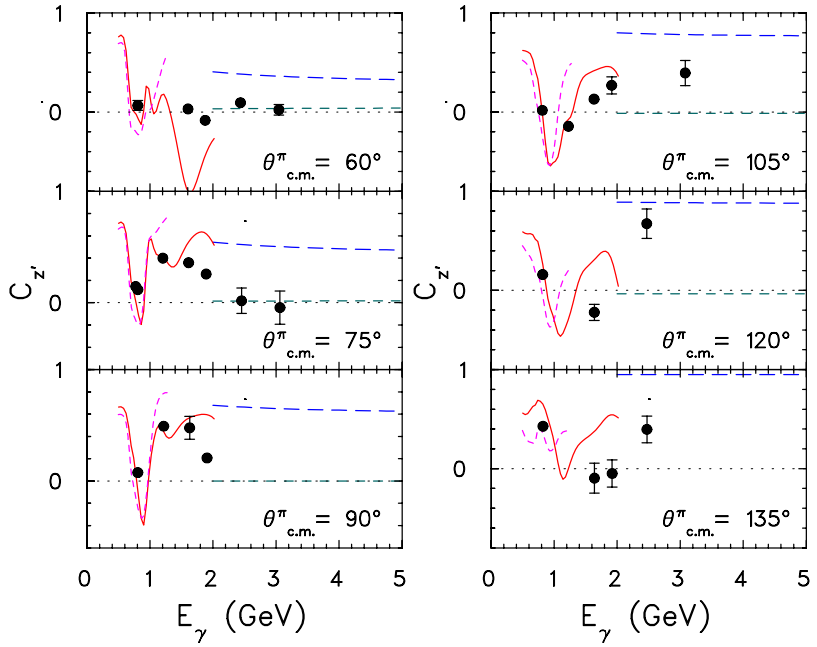

FIG. 1: Comparison of data and calculations for $C_{z'}$ in the lab frame. The solid and short dash curves at lower energies are the SAID and MAID partial wave analyses. The long dash curves at higher energies use polarization transfer to a quark, from Afanasev *et al.* [2]. The short dash curves at higher energies are pQCD calculations from Farrar *et al.* [3].

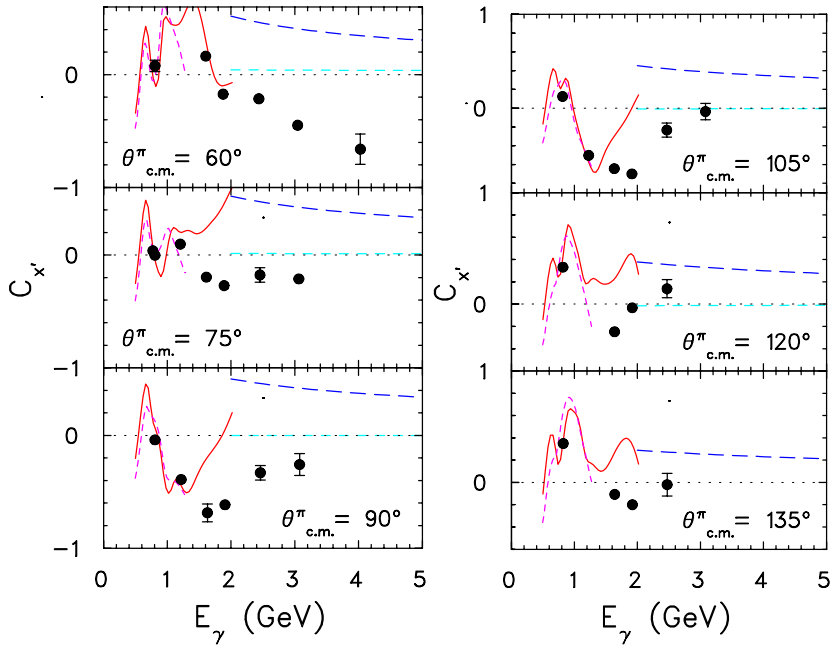

FIG. 2: Comparison of data and calculations for $C_{x'}$ in the lab frame. The solid and short dash curves at lower energies are the SAID and MAID partial wave analyses. The long dash curves at higher energies use polarization transfer to a quark, from Afanasev *et al.* [2]. The short dash curves at higher energies are pQCD calculations from Farrar *et al.* [3].

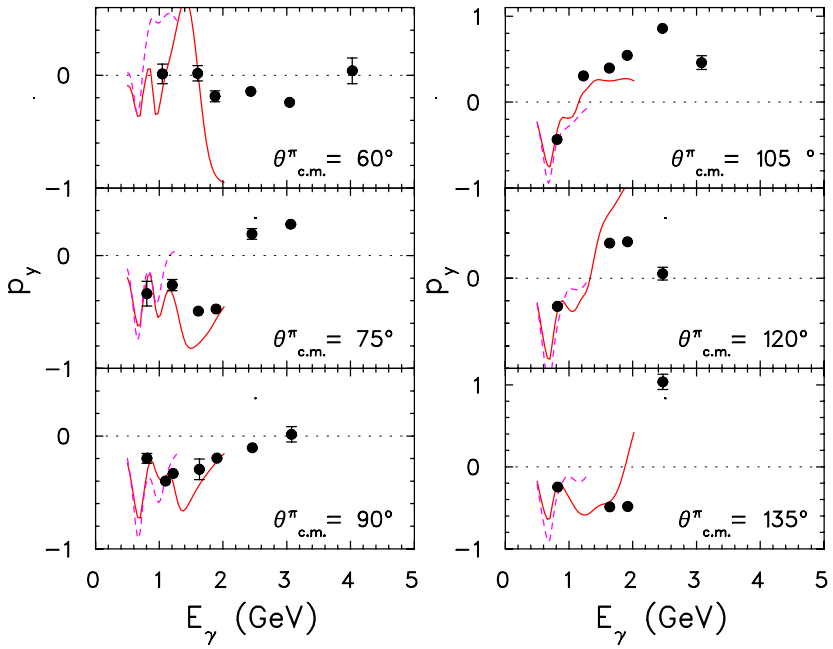

FIG. 3: Comparison of data and calculations for p_y in the lab frame. The solid and short dash curves at lower energies are the SAID and MAID partial wave analyses.

The recoil polarization data, in the lab frame, are shown in Figs. 1, 2, and 3. The choice of the lab frame is motivated by the following consideration: transforming the data to the usual c.m. frame mixes the x' and z' components. In some case, we have large (small) uncertainties on the lab z' (x') component; the boost can give two components with large uncertainties on both, which is not helpful in making a comparison with theory. It is instead better to transform the boost to the lab frame.

Our lower energy data, $E_\gamma < 2$ GeV, exhibit structures that were generally consistent with the SAID [4] and MAID [5] phase shift analyses, but sufficiently different to provide important constraints on background amplitudes, and to help clear up some observed anomalies in outlier points in some other observables. At higher energies, up to $E_\gamma = 4$ GeV ($W = 2.9$ GeV), the recoil proton polarizations continue to exhibit interesting angle and energy dependences; they do not approach a smooth or simple behavior, as we will discuss further below. In particular, the induced polarization is large, and even appears to be strongly oscillating with angle near 2.5 - 3 GeV beam energy. Hadron helicity conservation, a simple expectation from the vector coupling of photon to quarks, leads to the induced polarization, and $C_{x'}$, vanishing; it is not supported by the data. But as there are significant problems in understanding the helicity non-conserving amplitudes, they are generaly left uncalculated in most quark models.

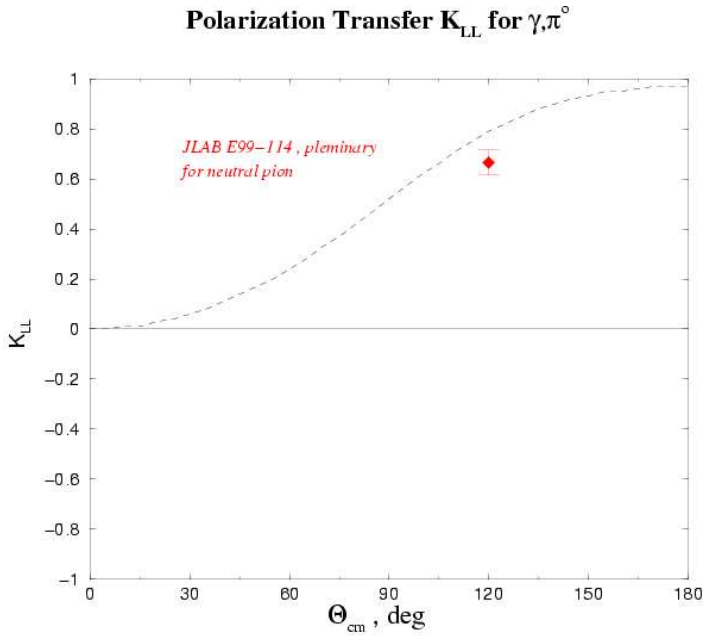

FIG. 4: K_{LL} measurement for $\gamma p \rightarrow p\pi^0$ background from the RCS experiment, compared to calculation of polarization transfer to a quark. The data were obtained at 3.2 GeV beam energy and a pion c.m. scattering angle of 120°.

Figure 4 shows another higher energy data point for $\pi^0 p$ photoproduction, taken as background during the RCS experiment, E99-114 [6]. Beam energy was 3.2 GeV. The data point is close to the calculation of polarization transfer to a quark, which smoothly increases with the pion angle. Given the data shown in Figs. 1, 2, and 3, this result might at first seem inconsistent and entirely fortuitous. But a closer look at these figures shows that the RCS data point is consistent with the trends from the lower energy data, and that there are indications of a trend of the larger energy, larger angle data to approach the helicity transfer to a quark calculation as the energy increases. Thus, the existing data set can be optimistically interpreted as being favorable towards the applicability of the GPD formalism at slightly higher energies.

GPDs

Understanding the quark structure of the nucleon is one of the prime goals of modern intermediate energy physics. There are many aspects to this problem, with numerous methods of investigation. The use of generalized parton distributions (GPDs) is of particular interest as it provides a unified description of nucleon structure, a common framework that can be applied to inclusive, semi-inclusive, and exclusive reactions. The use of GPDs requires investigation of the nucleon at large momentum transfer, so that the reaction description factorizes into two parts, a hard perturbative process and soft nucleon structure physics parameterized by the GPDs. The primary reactions of interest to date has been the pure photo-reactions, in particular deeply virtual Compton scattering (DVCS), since these are believed to be describable with GPDs over a wide, accessible, kinematic range. Measurements of nucleon form factors and real Compton scattering (RCS) are highly desirable, experimen-

tally simple, and described by GPDs, but they only involve moments of the GPDs, and thus do not have the capability to exhibit the kinematic dependences, as do DVCS or DDVCS.

Fully probing the GPDs requires however a more extensive set of measurements, going beyond the pure photo-reactions in particular to meson production reactions. Factorization has been theoretically proven most notably for high-Q^2, small-t, longitudinal ρ (and other vector) meson electroproduction. While there are some indications from experiments that longtidunal ρ electroproduction dominates over transverse electroproduction [7], σ_L/σ_T is only about 2 at JLab kinematics, so precise measurements of the longitudinal response will be difficult.

Here we propose to study the photoproduction of π^0 mesons, at energies of about 5 GeV. A form of factorization applies to the large $-t$, $Q^2 = 0$, photoproduction, and allows the process to be described using GPDs. Thus, the study of large momentum transfer photoproduction is just as important as the study of deep virtual meson production, for probing the handbag mechanism and GPDs. In similar kinematics, one expects handbag dominance to be similarly valid for the two types of reactions – if deep virtual meson production is described by GPDs, then the approach will also describe hard meson photoproduction. Hard π^0 photo-production is a particularly attractive reaction in which to study GPDs, as its large cross section allows both cross sections and polarizations to be measured over a wide kinematic range.

Measuring meson photoproduction is comparable to measuring the form factors or RCS in the case of pure photo-reactions. The photoproduction observables depend on moments of the GPDs. Pseudscalar meson production probes the $\langle x^{-1} \rangle$ moments of the GPDs. The most thorough study of pion photoproduction using the handbag mechanism and GPDs is by Huang, Jakob, Kroll, and K. Passek-Kumerički [8].

Meson photoproduction depends on three of the GPDs through form factors:

$$\begin{aligned} R_V^a(t) &= \int_{-1}^{1} \frac{dx}{x} \, \mathrm{sign}(x) \, H^{\,a}(x,0;t) \,, \\ R_A^a(t) &= \int_{-1}^{1} \frac{dx}{x} \, \widetilde{H}^{\,a}(x,0;t) \,, \\ R_T^a(t) &= \int_{-1}^{1} \frac{dx}{x} \, \mathrm{sign}(x) \, E^{\,a}(x,0;t) \,. \end{aligned} \tag{1}$$

There is no dependence on the GPD $\widetilde{E}$. The tensor form factor R_T^a is suppressed by a factor of $\Lambda/\sqrt{-t}$ compared to the vector and axial vector form factors, R_V^a and R_A^a. The R form factors conserve quark helicity (but not nucleon helicity); there is an additional set of corresponding quark helicity non-conserving form factors:

$$\begin{aligned} S_T^a &= \int_{-1}^{1} \frac{dx}{x} \, \mathrm{sign}(x) \, H_T^a(x,0;t) \,, \\ S_S^a &= \int_{-1}^{1} \frac{dx}{x} \, \mathrm{sign}(x) \, \widetilde{H}_T^a(x,0;t) \,, \\ S_V^a &= \int_{-1}^{1} \frac{dx}{x} \, \mathrm{sign}(x) \, E_T^a(x,0;t) \,. \end{aligned} \tag{2}$$

S_V^a and S_S^a are suppressed compared to S_T^a, but there is no particular reason why S_T^a is suppressed compared to R_V^a.

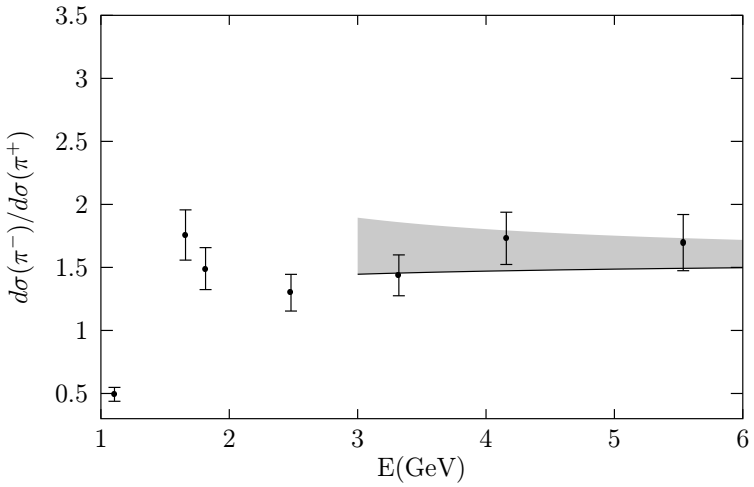

FIG. 5: The ratio of the $\gamma n \to \pi^- p$ cross section to that of $\gamma p \to \pi^+ n$, as a function of photon energy. Data are from [9]. The calculation is from [8]; The shaded band indicates uncertainties from target mass corrections.

For numerical calculations, the GPDs are modeled[1] in a conventional form as

$$\begin{aligned} H^a(x,0;t) &= \exp\left[a_N^2 t \frac{1-x}{2x}\right]\left[q_a(x) - \bar{q}_a(x)\right], \\ \widetilde{H}^a(x,0;t) &= \exp\left[a_N^2 t \frac{1-x}{2x}\right]\left[\Delta q_a(x) - \Delta\bar{q}_a(x)\right], \end{aligned} \tag{3}$$

with $a_N = 0.8$ GeV. Also, R_T is modeled as being related to R_V through

$$\kappa_T^P = \frac{\sqrt{-t}}{2m}\,\frac{R_T^P}{R_V^P}. \tag{4}$$

The ratio of the two form factors at high $-t$ falls similarly to the proton ratio of proton elastic form factors, F_2/F_1.

One result of the GPD calculation is for the ratio of π^+ and π^- photo-production cross sections, shown in Fig. 5, taken from [8]. The cross section ratio is given approximately by

$$\frac{d\sigma(\gamma n \to \pi^- p)}{d\sigma(\gamma p \to \pi^+ n)} = \left(\frac{e_u s + e_d u}{e_u u + e_d s}\right)^2, \tag{5}$$

in good agreement with the observed data. This agreement is also taken as evidence that the quark helicity consering matrix elements dominate. In particular, the helicity amplitudes can be expressed in terms of invariant functions, and the helicity conserving fuction C_2^p appears to dominate over the the helicity conserving fuction C_3^p and the the helicity non-conserving fuctions C_1^p and C_4^p.

Predictions are also available for some of the spin oberservables in $\gamma p \to \pi^0 p$. Assuming the dominance of C_2^p,

$$A_{LL}^P = K_{LL}^P \simeq \frac{s^2 - u^2}{s^2 + u^2}\,\frac{R_A^P}{R_V^P}\,(1 + \beta\,\kappa_T^P), \tag{6}$$

[1] An improved parameterization has been determined from the nucleon form factors [10].

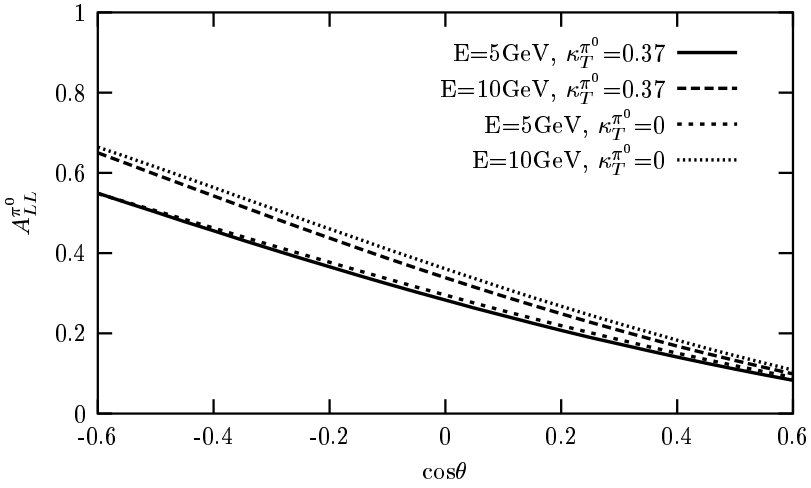

FIG. 6: Predictions for A_{LL} in $\pi^0 p$ photoproduction as a function of $\cos\theta$ for two beam energies and two values of $\kappa_T^{\pi^0}$, assuming the dominance of the $C_2^{\pi^0}$.

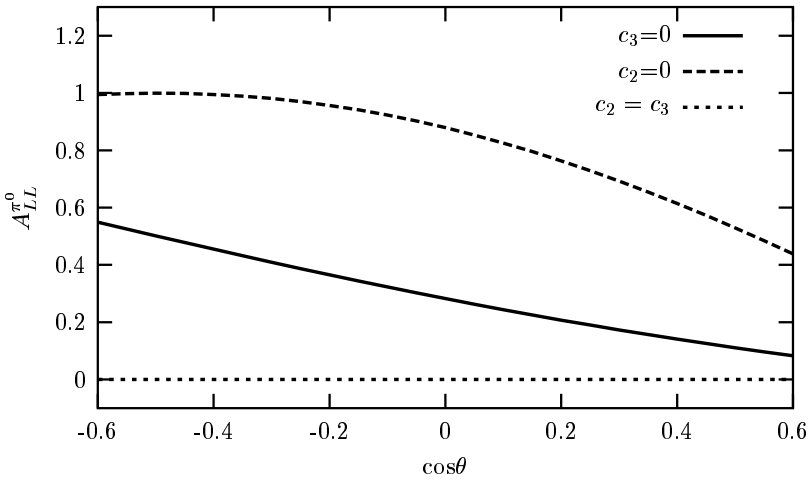

FIG. 7: Predictions for A_{LL} in $\pi^0 p$ photoproduction as a function of $\cos\theta$ at 5 GeV. The calculations use $\kappa_T^{\pi^0} = 0.37$.

with the equality of A_{LL}^P and K_{LL}^P coming from helicity conservation. The kinematic factors in front represent polarization transfer to a quark. For *real Compton scattering*, the single measured point for K_{LL} indicates that the remaining kinematic factors are close to unity [11] – $R_A/R_V = 0.81 \pm 0.11$ – for $s = 6.9$ GeV^2 ($E_\gamma = 3.5$ GeV) and $-t = 4$ GeV^2.

Several predictions for the helicity correlation $K_{LL} = A_{LL}$ are shown in Figs. 6 and 7, again taken from [8]. Figure 6 shows that under the assumption of C_2 dominance, the resulting polarization transfer has only small dependences on the parameter $\kappa_T^{\pi^0}$ and on the beam energy. Figure 7 shows that a wide variety of smooth behaviours can be accomodated by the handbag mechanism, if one allows contributions from both C_2 and C_3, but generally one expects the longitudinal polarization transfer to be positive, and to vary smoothly with

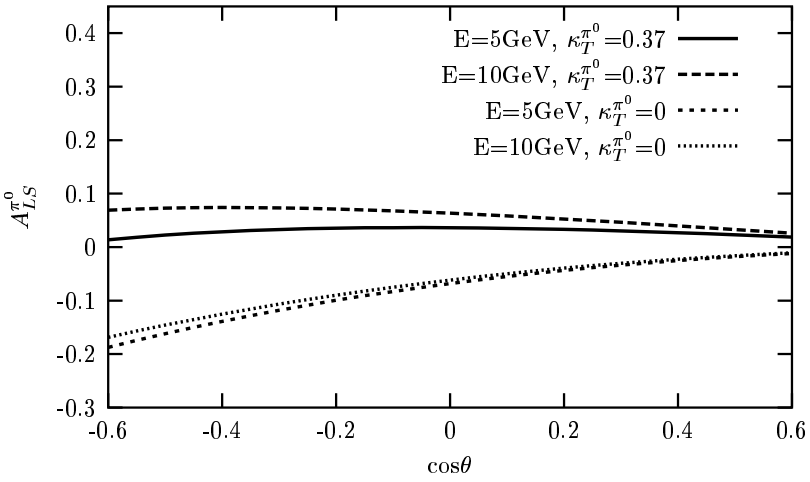

FIG. 8: The longitudinal - transverse spin observable A_{LS} for π^0 photoproduction. Curves are the same as for Fig. 6.

angle.

The longitudinal - transverse polarization transfer, $A_{LS} = -K_{LS}$ is also predicted in [8]. If $C_2^P \gg C_3^P$, they find

$$A_{LS}^P \simeq \frac{s^2 - u^2}{s^2 + u^2} \frac{R_A^P}{R_V^P} \left(\kappa_T^P - \beta\right), \tag{7}$$

which depends in the difference of two small terms, rather than one plus a small term. The calculations are shown in Fig. 8. Although the only calculations shown assume C_2 dominance, it appears reasonable to conclude that the handbag mechanism can accomodate a variety of results showing a smooth behavior, with K_{LS} small and of either sign.

An important result is that the ratio of the polarization transfer components, given by

$$\frac{K_{LS}^P}{K_{LL}^P} = -\frac{A_{LS}^P}{A_{LL}^P} = -\frac{\kappa_T^P - \beta}{1 + \beta\kappa_T^P}, \tag{8}$$

is the same for both $\pi^0 p$ photoproduction and from real Compton scattering. This result is independent of C_2 and C_3. The calculations of [8] indicate that the ratio is small. The RCS experiment [11] finds it to be 0.17 ± 0.12 in their kinematics, 3.2 GeV and 120°.

From Eqs. 6 and 7, one can see that if the GPD formalism applies, in each of our kinematic points we can extract the form factor ratios R_A^P/R_V^P and R_A^P/R_V^P from the polarization transfer observables. By simultaneously measuring the cross sections, we can determine the absolute magnitudes of these form factors.

While the existing data are at too low of an energy to be described by GPDs, as we have indicated above, an examination of Figs. 1, 2, and 3 might be interpreted optimisitically as promising for the applicability of the GPD formalism at slightly higher energies. Thue, we expect at high energies that $C_{x'}$ and p_y are small, while $C_{z'}$ is large, similar to the calculated polarization transfer to a quark. To conclude this discussion of the handbag mechanism and GPDs, we quote from [8]: *At JLAB the observables K_{LL} and K_{LS} have recently been measured for π^0 photoproduction [1] in a kinematical range however in which the handbag*

approach cannot be applied. Measurements of these observables at higher energies are needed. **These measurements are the goal of this proposal.**

Resonances and duality

Inclusive (e, e') has been used to investigate nucleon resonances and duality, the averaging of resonances to the corresponding deep-inelastic scattering result, for many years; duality has been found to work very well for cross sections. In the recent past, electromagnetic studies have turned to whether duality also holds for the spin-dependent cross sections, and neutrino studies are planned to investigate whether duality holds for the weak interaction.

These ideas can also be applied to exclusive reactions. It has long been known that high-energy meson photoproduction reactions exhibit a more or less smooth power-law dependence[2] that approximately follows the constituent counting rules. We now better understand that this behaviour can not be simply interpreted as evidence for perturbative quantum chromodunamics, as the GPD picture provides similar predictions, with small scaling violations unobservable in the early data. These observation, combined with the non-smooth behavior that we observed in the recoil polarizations, make it tempting to speculate that highly excited baryon resonances, in the hadronic picture, are averaging to a quark model behavior, but only for the cross sections. Thus, there is a duality in the exclusive reaction cross sections, but not in the spin observables. That is, while we might not know what is the apprpriate quark model picture, we expect that it leads to some smooth energy and angle dependence, as it lacks the interfering mechanisms that generate structures.

pQCD and helicity conservation

It was for many years believed that pQCD led directly to hadron helicity conservation. A more modern view, championed for many years by Ralston and colleagues [12], is that orbital angular momentum is always important and helicity conservation will generally not be observed in reactions with hadrons. Our measured neutral pion photoproduction data [1] go well above 2 GeV, the nominal limit of the resonance region, but continue to exhibit strong energy and angle dependences. Helicity conservation has a clear prediction: the observables $C_{x'}$ and p_y must vanish. Helicity conservation does not constrain $C_{z'}$. The data shown in Figs. 1, 2, and 3 clearly indicate non-vanishing, even large, polarizations for $C_{x'}$ and p_y. Thus it is clear that helicity conservation was not seen.

If helicity conservation were to hold, what is expected for $C_{z'}$? There is a clean prediction for polarization transfer to a quark:

$$C_{z'} = \frac{s^2 - u^2}{s^2 + u^2} \tag{9}$$

The several estimates made which respect helicity conservation are basically similar to this simple expression, though wave function effects tend to dilute the polarization.

[2] There are some indications of possible oscillations in the high energy cross sections, leading to the suggestion that, as for the case of *pp* elastic scattering, there exists a nonperturbative QCD process of similar size but different phase interfering with the pQCD amplitude.

Regge Theory

A Regge theory model has been formulated and applied to the world data for pseudoscalar meson photoproduction above the resonance region [13]. Large $-t$ cross section data are sparse and not very precise, but are reasonably well represented as a sum of t and u channel exchanges in the model. There are a number of polarization measurments over a range of energies, but all at low $-t$, below about 1 GeV^2, and forward angles. These data are also qualitatively reproduced. Naively extrapolating the Regge theory polarization calculations to higher $-t$, one expects polarization effects to smoothly vanish.

$K^+\Lambda^0$ production

There is a sharp contrast between the $p\pi^0$ photo-production data from Hall A and the $K^+\Lambda^0$ production data from Hall B [14, 15]. Hall B data on recoil spin observables in $K^+\Lambda^0$ electro-production and photo-production have exhibited a very simple behavior, but one that is unrelated to any of the simple behaviors generally mentioned for pseudoscalar meson production. The spin of the Λ^0 is oriented approximately in the direction of the photon spin. This behavior was observed over the entire measured kinematic range. We have subsequently re-examined the $\vec{\gamma}p \to \pi^0\vec{p}$ data to see if this simple behavior is exhibited in that reaction; it is not. The structures seen in the data persist when converting from lab frame to the "photon frame" [16].[3]

The $K^+\Lambda^0$ data have been interpreted as possibly indicating that the production of a quark-antiquark pair from the vacuum, in this case an $s\overline{s}$ pair, happens in a state with $S = 0$. Alternate production reactions, such as pion photoproduction, can illuminate the underlying physics. The observations in $K^+\Lambda^0$ production might result from constraints of the simpler spin structure of the Λ^0 wave function, as compared to the nucleon wave function. If the complicated behavior of the lower energy $\pi^0 p$ photo-production reflects important resonance effects, then it is necessary to measure at higher energies, both to see if the data exhibit smaller, perhaps vanishing, resonance effects, and to see whether they approach the same simple behavior exhibited by the $K^+\Lambda^0$ data.

Motivation Summary

There is at present a lack of understanding of the underlying physics of multi-GeV pion photoproduction. Our goal is to provide a detailed data set to allow the underlying physics mechanism to be identified, and so that we can get insight into the structure of the nucleon at large W and $-t$.

The ideas discussed lead to several quite distinct possibilities for the high energy recoil proton polarizations. We are optimistic, based on the hints of trends in the lower energy data, that the polarization observables will approach the predictions from the GPD formalism: $C_{x'}$ will be small, but not vanishing, indicating helicity non-conservation, and $C_{z'}$ will reflect

[3] Note that the transformation is not simply a rotation by the scattering angle. Relativistic boost effects lead to an additional spin precession. The angle between the photon and the recoil baryon momentum is different in the lab, c.m., and baryon rest frames.

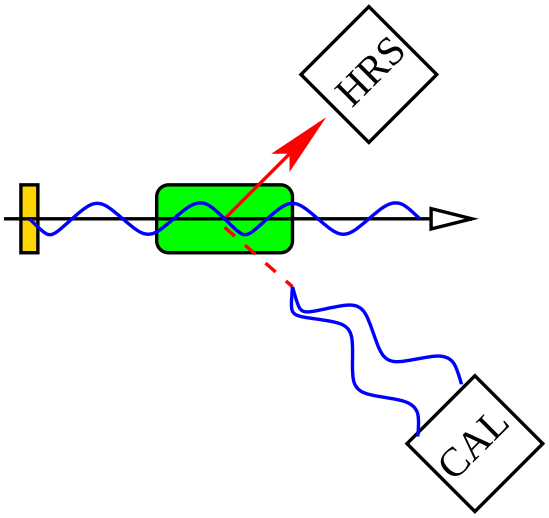

FIG. 9: The planned experimental configuration. See text for details.

the calculated polarization transfer to a quark, reflecting the importance of the handbag mechanism. The induced polarization will also be small. Once this behaviour is established, the polarization observables and the cross sections can be used to extract the generalized "R" form factors from the data.

We can not guarantee that this behaviour will actually be observed. We have mentioned above other possiblilites. There might be a continuation of the strong energy and angle variations of the polarization observables, as observed at lower energies, indicating a continuation of important resonance contributions. Or these might be other behaviors, such as the proton spin might point in the photon spin direction

Our nearest similar experience to these measurements is the Hall A RCS measurements. For these, the fall of the cross sections with energy generally agrees with Radyushkin's handbag predictions, while the single recoil polarization point at 3 GeV is consistent with Huang and Kroll's handbag predictions. We propose to measure π^0 photoproduction at larger W and $-t$ so that the momenta carried by each quark are similar. Thus we are optimistic that the same underlying physics picture also holds.

EXPERIMENT

Overview of Technique

An overview of the experimental setup is shown in Fig. 9. We use a 6% radiator to generate a mixed photon plus electron beam that strikes the target. Protons exiting the target are detected in the HRS spectrometer, with the focal plane polarimeter (FPP) determining their polarization. The coincident π^0 decays essentially immediately, and the two decay photons are detected in the BIGCAL calorimeter.

Our previous Hall A $\gamma p \rightarrow p\pi^0$ experiment [1] also used the CEBAF electron beam incident on a 6% copper radiator to produce an untagged Bremsstrahlung photon beam. We detected singles protons in the hadron HRS, and used the FPP to determine their polarization. The measurements were performed in the kinematically clean region, within

TABLE I: Helicity amplitudes for pseudoscalar meson photoproduction.

Spin flip (h not conserved)	Non spin flip (h conserving)
$D = \langle \frac{-1}{2} 0 \vert T \vert 1 \frac{1}{2} \rangle$	$S_1 = \langle \frac{1}{2} 0 \vert T \vert 1 \frac{1}{2} \rangle$
$N = \langle \frac{1}{2} 0 \vert T \vert 1 \frac{-1}{2} \rangle$	$S_2 = \langle \frac{-1}{2} 0 \vert T \vert 1 \frac{-1}{2} \rangle$

$\approx$ 100 MeV of the photon endpoint[4].

The problem with these singles measurements is that as energy and proton angle increase, the $ep \rightarrow ep$ elastic scattering background increases relative to the desired signal and becomes harder to separate. To improve the situation, we now propose to make use of the technique employed by the Hall A RCS experiment [6]: we use a calorimeter to detect the coincident photons. The RCS experiment also used a sweeping magnet – not shown in Fig. 9, as we do not plan to use it – to deflect outgoing electrons, so that the $\gamma p \rightarrow \gamma p$ channel could be separated from $ep \rightarrow ep$ background channel. In addition, because both outgoing particles were detected, the experiment could be run cleanly with kinematics for photons at energies several hundred MeV below the photon end point.

With the calorimeter close enough to the target, we can detect both of the two outgoing photons from the $\pi^0 \rightarrow \gamma\gamma$ decay (99.8 % branching ratio). Although the decay photons cover 4π in the laboratory, the boost concentrates the phase space so that we can capture both decay photons with about 50 % efficiency. The benefits of using the calorimeter and measuring away from the bremsstrahlung end point include increased photon flux and rates, reduced backgrounds, improved uncertainties for fixed beam time, and the ability to run with a range of electron energies. Removing the dominant ep and γp backgrounds allows a clean measurement of the pion photoproduction recoil proton polarization, while simultaneously allowing us to identify a clean sample of ep elastic events to use to calibrate the proton polarimeter and the photon calorimeter. Brief tests done during the RCS experiment indicate that clean measurements of the type proposed here can be done over a wide range of photon energies, down to perhaps half the beam energy.

Previous measurements of $\pi^0 p$ photo-production have generally used either singles protons or the proton in coincidence with one decay photon. By measuring both decay photons, we will have the cleanest measurements possible at the highest momentum transfers. This will allow us to measure absolute cross sections with small uncertainties. It is important to recall that our statistics are determined by the need to measure good polarizations. This means that typically we will obtain of order 1 million pion photproduction events. Because we use the calorimeter, we will also be able to derive cross sections based on the calorimeter geometry, using only a small fraction of the acceptance, determined purely from geometry. This reduces systematic uncertainties. Thus, we can subdivide our data set into numerous small bins with < 1 % statistics, for precise studies of the variation of the cross section within each spectrometer setting.

[4] The number given is approximate; the exact limit varied by about a factor of two and depends on the energy and angle.

TABLE II: Observables of this proposal.

Observable	Formula
$d\sigma/dt$	$N^2 + S_1^2 + S_2^2 + D^2$
$p_y d\sigma/dt$	$2\Im(S_2 N^* - S_1 D^*)$
$C_{x'} d\sigma/dt$	$-2\Re(S_2 N^* + S_1 D^*)$
$C_{z'} d\sigma/dt$	$S_2^2 - S_1^2 - N^2 + D^2$

Observables and Helicity Amplitudes

In this section, we review the pseudoscalar meson photoproduction observables, and give the helicity amplitudes for them. We also show the implications of various assumptions about the amplitudes on the observables. We follow the notation of [17].

Pion photoproduction is described by four complex helicity amplitudes. With one overall phase, there are seven independent parameters. The four helicity amplitudes are labelled N, D, S_1, and S_2, referring to nonflip, double flip, and single flip of the total helicity between initial and final states. The amplitudes $\langle \lambda_{p'} \lambda_{\pi^0} | T | \lambda_\gamma \lambda_p \rangle$ are given in Table I. Expressions for the observables that we propose to measure are given in Table II. Note that the observables K_{LL} and K_{LS} in the GPD predictions of [8] are the same as the observables $C_{z'}$ and $C_{x'}$ in the notation of [17].

The coordinate is chosen with x, y, and z aligned according to the initial state momenta, and x', y', and z' aligned according to the final state momenta. The out-of-reaction plane coordinate unit vector is $\hat{y} = \hat{y}'$. In the initial state, $\hat{z}$ is along the photon momentum, and $\hat{x}$ is in-plane and transverse to the photon momentum, so that $\hat{x} \times \hat{y} = \hat{z}$. In the final state c.m., $\hat{z}'$ is chosen to be in the meson direction. This is unnatural from the recoil proton polarization point of view, and requires a negative sign in the definition of $C_{z'}$ so that one obtains the intuitive behavior: positive $C_{z'}$ indicates a proton polarized parallel to its momentum direction. Then $\hat{x}' = \hat{y}' \times \hat{z}'$. This unnatural choice of c.m. coordinate system (from the recoil proton polarization perspective) leads to a variety of definitions of the recoil lab system, and corresponding consistent transformations between the two frames.

Hadronic helicity conservation requires that $\lambda_{p'} = \lambda_p$, leading to $N = D = 0$. Thus, the observables p_y and $C_{x'}$ vanish. The remaining two observables are sufficient to uniquely determine the magnitudes, but not the relative phase, of the amplitudes S_1 and S_2, with $S_1^2 = d\sigma/dt \times (1 + C_{z'})$, and $S_2^2 = d\sigma/dt \times (1 - C_{z'})$.

If the amplitudes are real, as would be expected in a GPD model without explicit gluon lines, then p_y vanishes, and the four amplitudes are constrained by the three non-vanishing observables that we measure.

Chiang and Tabakin [18] provided the definitive solution to the problem of uniquely determining the amplitudes from limited sets of observables; they found that eight properly chosen observables can uniquely determine the reaction amplitudes. An additional important point is that there is no new information in triple spin observables, as these are entirely redundant with simpler double spin measurements. This proposal cannot uniquely determine the amplitudes. Note that there are existing Hall B experiments that attempt to uniquely determine the amplitudes for low energy $\pi^0 p$ and $K^+\Lambda^0$ photo-production, using polarized beams and targets. The recoil polarization observables that we propose to measure here are

TABLE III: Proposed kinematics. E_γ = 5 GeV, s = 10.3 GeV^2, and W = 3.2 GeV.

$\cos\theta^\pi_{cm}$	-0.4	-0.2	0.0	0.2	0.4	0.6
θ^π_{cm} (deg)	113.58	101.54	90.0	78.46	66.42	53.13
θ^π_{lab} (deg)	47.98	39.31	32.54	26.82	21.65	16.62
p^π_{lab} (GeV)	1.80	2.26	2.72	3.17	3.63	4.09
θ^p_{lab} (deg)	19.44	23.76	28.33	33.43	39.46	47.13
p^p_{lab} (GeV)	4.02	3.55	3.07	2.60	2.11	1.59
t (GeV^2)	-5.99	-5.13	-4.28	-3.42	-2.57	-1.71
u (GeV^2)	-2.49	-3.35	-4.21	-5.06	-5.92	-6.77
p_T (GeV)	1.34	1.43	1.46	1.43	1.34	1.17

not measured in the Hall B $\pi^0 p$ experiment, nor do these Hall B experiments include the high energy, large angle kinematics.

Choice of Kinematics

Our goal of measuring well above the resonance region, so that the handbag mechanism and GPDs likely describe the underlying physics, requires beam energies near 5 GeV (W $\approx$ 3.2 GeV). As twe operate off the Bremsstrahlung end point, the most likely scenario is that we would use a 5-pass 5+ GeV electron beam, and center the acceptance of our measurements for about 5 GeV photons. Due to the fast fall off of the cross sections with energy, we would not operate much above 5 GeV.

The lower energy data [1], near 3 GeV, indicate that the observables might vary rapidly with scattering angle. In particular, one sees that p_y at 2.5 GeV goes from near 1 to near 0 in 15°. Thus, we need to measure several angles, over a wide range of scattering angles, to be sure that there is no fine structure to our data. Experience from the RCS experiment suggests that angle changes of the calorimeter can be accomplished in about 2 hours, which is only slightly longer than it takes to simply move the HRS spectrometer and cycle the magnets.

At 5 GeV photon energy, the experimentally accessible range of $\cos\theta^\pi_{cm} \approx$ -0.42 $\rightarrow$ 0.64 approximately coincides with the range calculated by [8], $\cos\theta^\pi_{cm}$ = -0.6 $\rightarrow$ 0.6. Thus, to largely cover the calculated range, to test the GPD prediction but with fine enough spacing to look for high-frequency behavior, we request six measurements, evenly spaced at $\cos\theta^\pi_{cm}$ = -0.4, -0.2, 0.0, 0.2, 0.4, and 0.6. The kinematics are shown in Table III. It can be seen that the momentum transfers are large, well above 1 GeV^2 in magnitude, for Mandelstam t and u. The transverse momentum also exceeds 1 GeV. The acceptance of the HRS spectrometer, ±1.5°, combined with the angles selected, gives us nearly continuous coverage of the angular range, particularly for backward pion angles. These settings can also be binned into finer settings (although with reduced statistical precision) to check for high frequency behavior, rapid variation of the polarization observables with angle, which can result from interfering amplitudes.

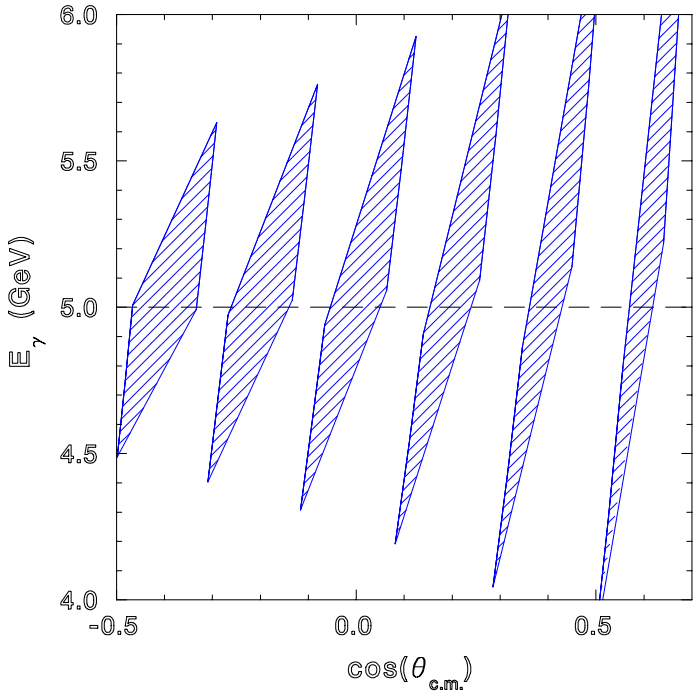

FIG. 10: The acceptance limits of the measurements as determined from the HRS arm detecting the proton.

HRS Coverage

In taking data for the experiment, a single proton setting covers a range of incident photon energies and scattering angles. Using Table III along with the $\approx 3^\circ$ horizontal acceptance of the spectrometer, it can be determined that the angle coverage is nearly continuous for backward π^0 angles, decreasing to about 40 % coverage for the forward π^0 angles.

The coverage in photon energy is less clear, but it is typically several hundred MeV. Fig. 10 shows the range of coverage of E_γ as a function of $\cos\theta^\pi_{cm}$. It can be seen that as the pion angle increases, one has better coverage in photon energy, but less coverage in angle. Note that these are the acceptance limits – the solid angle acceptance smoothly goes to 0 at the limits of the displayed regions. Also, note that for the forward pion angles in particular the acceptance extends above the bremsstrahlung end point.

Calorimeter

During this experiment we plan to use only two-photon events in a calorimeter to identify the outgoing π^0. A drawing of the BIGCAL calorimeter is shown in Fig. 11. The calorimeter is being built by Halls A and C for several already approved experiments. It will initially be used in the Hall C G^p_E-III experiment; it is also planned to use it in the Hall C SANE experiments and the Hall A RCS-II experiment, E03-003. The calorimeter technique has already been used in Hall A during the G^p_E-II experiment [19] and during the RCS experiment [6], which operated more similarly to the conditions of this proposal.

A sample π^0 background event from the RCS experiment is shown in Fig. 12. The identification of this event is confirmed by the positions and energies of the two clusters.

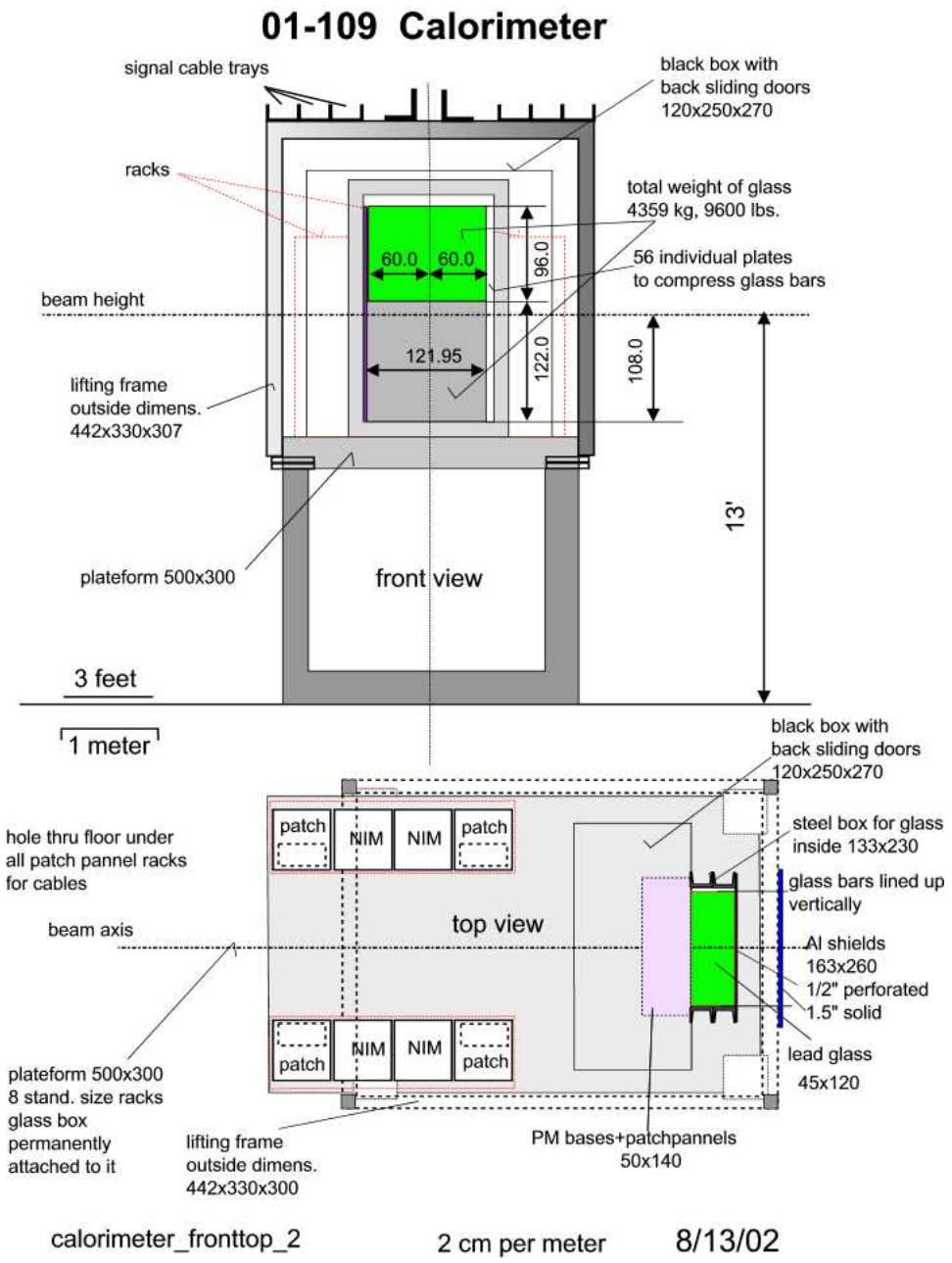

FIG. 11: A plan drawing of the BIGCAL calorimeter, as it is being implemented for the Hall C G_E^p-III experiment. The calorimeter face is approximately 1.2 m wide by 2.2 m tall. The calorimeter contains 1744 lead-glass crystals.

A 1-GeV π^0 with decay photons in the c.m. at angles of 60° and 120° gives two photons with energies of 750 MeV and 250 MeV in the lab, and an opening angle of 18° in the lab. This leads to a 1.3 m separation in the calorimeter between the two energy clusters. The energies and spacing in the event display are consistent with these numbers, so we see that this is a π^0 decay event.

It is evident that this technique allows a clean identification of the outgoing π^0, since background hits in the calorimeter tend to have small energy. In the $\approx$ 600 blocks of the

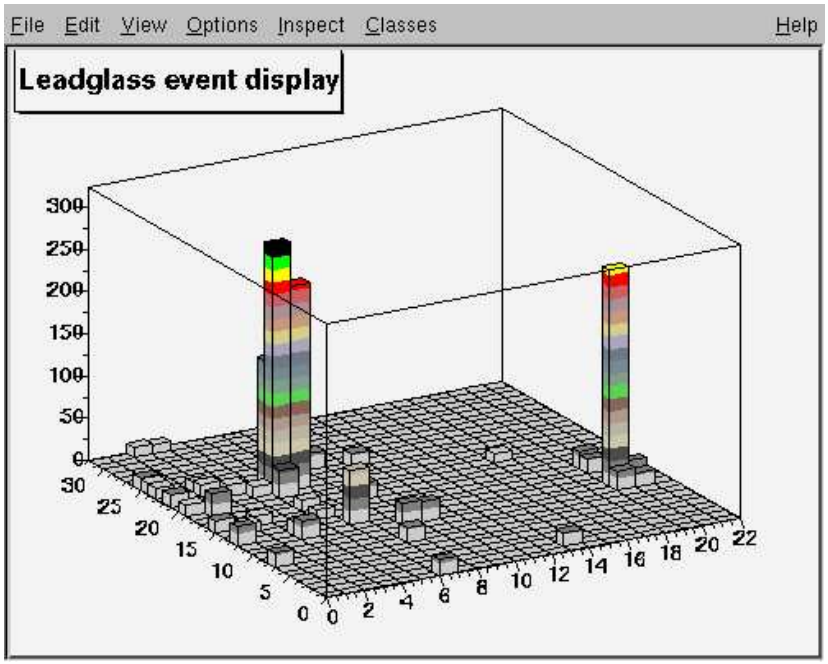

FIG. 12: An event from the RCS experiment, showing two photons from a $\approx$ 1 GeV π^0 decay plus random background. The beam energy was 3.5 GeV. The calorimeter was 4 m from the target, at a lab angle of 31°. Current was 3 μA incident on a 6 % radiator and a 15-cm long hydrogen cryotarget.

RCS calorimeter, there are, besides the two clusters, about a dozen other hits with energies of a few tens of MeV. The probability of such a hit in any block is around 2 %. As the low energy background is relatively isotropic, and as we measure π^0 with energies ranging from about 2 to 4 GeV, it is clear that we can run with much higher luminosities and still cleanly see the two-photon π^0 decay signal.

Using the calorimeter requires that it be calibrated. The calibration comes "for free" during the experiment, through the use of elastic *ep* data that is contained within the HRS spectrometer acceptance. These data allow us to calibrate both the calorimeter central angle and the energy.

The calorimeter settings for the experiment are shown in Table IV. The angle range determination includes the effects of the finite acceptance of the HRS spectrometer, which leads to a range of pion angles in and out of the reaction plane, along with the angles of the $\pi^0 \rightarrow \gamma\gamma$ decay. The opening angle for two photons at 90° c.m. decay angle gives a rough idea of the angle range that is needed to be covered. A better indication requires that we consider the c.m. decay angles of 60° and 120°, since this corresponds to $\cos\theta$ = -0.5 $\rightarrow$ 0.5, which is half of the decay phase space. The 120° c.m. photon is at a larger lab angle, and is used to determine the nominal photon angle range. The vertical and horizontal ranges change with angle at different rates due to kinematic effects.

The apparent angle ranges needed are crudely equal in the horizontal and vertical directions, but the calorimeter has about twice the vertical acceptance. Our plan is to position the calorimeter at an intermediate distance, so that we have access to large decay angles in the vertical direction, to make up for a loss of acceptance in the horizontal direction. The loss is not as large as it might seem. The vertical acceptence is determined by the reaction

TABLE IV: Calorimeter settings. The angle ranges are those needed to capture a $\theta_{c.m.} = 120^\circ$ decay photon from a pion corresponding to a proton in the HRS acceptance from a 5 GeV ± 50 MeV incident photon.

$\cos\theta^\pi_{cm}$	-0.4	-0.2	0.0	0.2	0.4	0.6
θ^π_{lab} (deg)	47.98	39.31	32.54	26.82	21.65	16.62
p^π_{lab} (GeV)	1.80	2.26	2.72	3.17	3.63	4.09
$\theta_{lab\,\gamma\gamma 90}$ (deg)	8.58	6.84	5.68	4.88	4.26	3.78
floor angle range (deg ±)	12.5	10.3	8.8	7.8	7.1	6.4
vertical angle range (deg ±)	15.5	11.5	8.9	7.0	5.7	4.6
Distance for horizontal match (m)	2.70	3.30	3.87	4.38	4.82	5.35
Distance for vertical match (m)	3.97	5.41	7.02	8.96	11.02	13.67
Planned calorimeter distance (m)	3	4	5	6	7	8

plane and angle between the π^0 and the backward going decay photon. The horizontal acceptence in contrast reflects the range of kinematics accepted by the HRS spectrometer. The spectrometers have a complicated acceptance function for extended targets, but the crucial feature is that the acceptance smoothly goes to 0, as opposed to having a sharp cut off, at the limits of the horizontal angular acceptance. Thus, the fraction of events lost is much smaller than the fraction of the horizontal acceptance that is lost.

For the decay $\pi^0 \to \gamma\gamma$, the fraction of the pion energy carried by the photon depends mainly on the photon angle in the rest frame – it is nearly independent of the pion energy. For the decay at 90°, the fractional energies are 0.5, while for the 60-120° decay, the energy fractions are 0.75-0.25. Thus, the 120° photon will have energies ranging from 0.45 - 1.0 GeV in the kinematics of this experiment. The expected resolution of the calorimeter is about $6\%/\sqrt{E}$, with the photon energy E in GeV. This corresponds to energy resolutions from 40 MeV at 0.45 GeV to 100 MeV at 3 GeV.

We use $W = \sqrt{2E_{\gamma_1}E_{\gamma_2}(1-\cos\theta_{\gamma\gamma})}$ to reconstruct the π^0 invariant mass from the two photons. The mass resolution is about 15 MeV, and is insensitive to the kinematics. Thus, there is good rejection of background events containing two photons that are either random or from the decay of a heavier meson. The invariant mass of two random photons ranges from about 0, for two minimally separated clusters or low energy photons, up to $W \approx \sqrt{2\times 4\times 4(1-\cos 45)} = 3.1$ GeV, for two high-energy photons in opposite corners of the calorimeter, at a distance of 3 m. Thus the acceptance is about 200 times the resolution.

FPP

We propose to use the now-standard dual-analyzer FPP in Hall A, to improve efficiencies. We have adopted this technique previously for the G^p_E-II, RCS, and deuteron photodisintegration experiments. A sample of dual analyzer data is shown in Fig. 13. It is clear that the two analyzers give the same azimuthal asymmetry shape - they are independent measurements of the same polarization. The benefit of the dual analyzer is that it nearly doubles the statistics of the experiments, at the cost of a few day installation period.

The FPP calibration will be checked by *ep* elastic scattering data, which is in the HRS

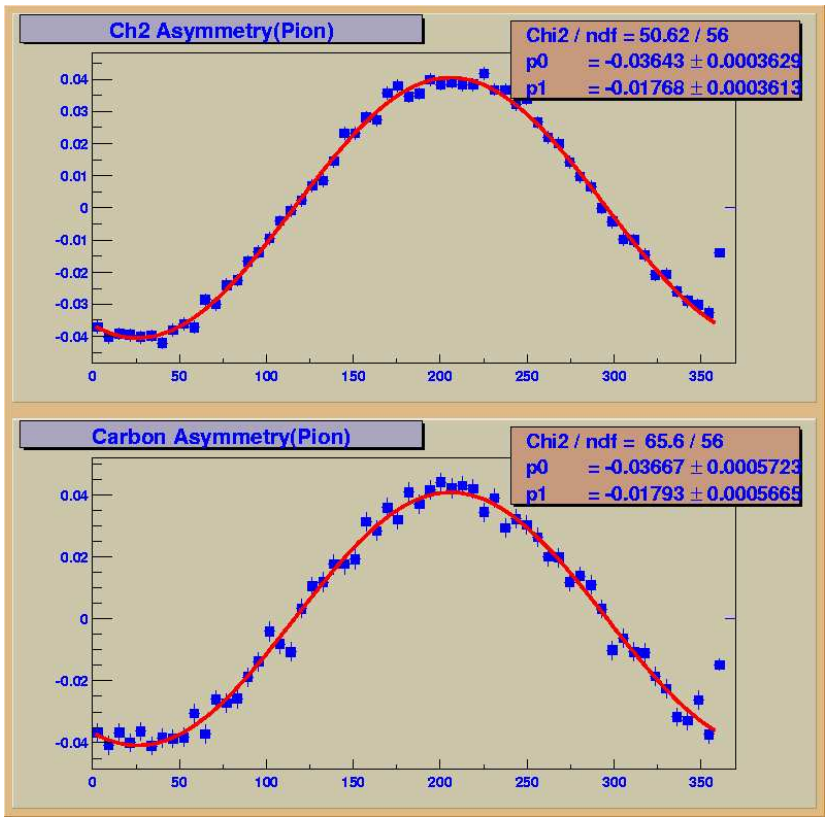

FIG. 13: Azimuthal scattering angle distributions from the measurement of recoil polarization in the $p\pi^0$ background to the RCS experiment.

acceptance. The uncertainty estimates are based on the efficiencies and analyzing powers that we have determined in previous experiments. While these vary with proton momentum, for the high momenta of this experiment the dual analyzer efficiency is nearly 50 % and the analyzing power is about 0.1. Our uncertainty estimates also include the effects of spin precession, using the leading order dipole spin transport.

Backgrounds

There are several potential backgrounds in the experiment. Most are elimated by the requirement of a coincidence between a high-energy proton in the HRS spectrometer and two photons, each with energy of order $E_\pi/2$, in the calorimeter.

Elastic ep protons are the highest momentum protons at each angle. We plan to make use of this background both to calibrate the FPP and the calorimeter. Singles events near the endpoint are dominated by ep elastic scattering; using a one-photon and calorimeter position cut allowed the G_E^p-II experiment to select $\geq$ 99 % pure ep elastic scattering. For the $p\pi^0$ photoproduction data, the ep background is elimated as there is a single cluster in the calorimeter, with energy about E_π[5]. The elastic radiative tail does not change this

[5] Recall that for these high energies, there is little difference between the kinematics of $ep \to ep$, $\gamma p \to \gamma p$, and $\gamma p \to \pi^0 p$.

TABLE V: Time request. Numbers given are for a 100 MeV bin in incident photon energy, centered at 5 GeV, covering the full spectrometer colid angle.

$\cos\theta^{\pi}_{cm}$	-0.4	-0.2	0.0	0.2	0.4	0.6
$d\sigma/dt$ (nb/GeV^2)	0.5	0.5	0.5	0.6	1.0	2.1
rate (Hz)	3.5	2.5	2.1	2.0	2.2	3.0
Time requested (days)	5	4	4	4	3	2
Δp_y^{lab}	0.03	0.06	0.22	0.07	0.03	0.02
$\Delta C_{x'}^{lab}$	0.04	0.05	0.05	0.05	0.03	0.03
$\Delta C_{z'}^{lab}$	0.15	0.07	0.05	0.06	0.11	0.08
spin boost mixing (deg)	19.5	23.8	28.4	33.5	39.6	47.3

conclusion.

Real Compton scattering is similarly rejected from the π^0 photoproduction data by the single, high-energy cluster in the calorimeter; While RCS events look like *ep* elastic scattering events, RCS event rates are much smaller.

Potential real physics backgrounds with multiple clusters in the calorimeter include multiple pion production, and production of heavier mesons, such as the η, which have two-photon, or multi-pion, decay channels. These backgrounds are highly suppressed. The two photons from η decay have a larger opening angle, are not usually both detected in the calorimeter, and will not reconstruct to the pion invariant mass. Production of two neutral pions, each of which decays into one forward and one backward going photon, could lead to a similar signal as the decay of one neutral pion. However, one immediately sees that the phase space for this background is small, and there is no reason to expect that the cross section for this channel is orders of magnitude above the cross section for single pion production.

The aluminum target walls also generate backgrounds. These backgrounds are suppressed by three factors. First, there are about 10 times as many hydrogen atoms in the target as there are nucleons in the aluminum walls. Second, the target reconstruction from the HRS proton data allows simple cuts that reduce the end cap contributions by about an order of magnitude. Third, nuclear effects reduce the cross section through absorption and rescattering effects, and through Fermi momentum which changes the kinematics correlations by of order a hundred MeV/c, typically a few degrees.

Time Estimates

The time request is shown in Table V; the total requested time is for 22 days. Our count rate estimates for $p(\vec{\gamma},\vec{p})\pi^0$ start from measured cross sections of [20]. Since there are only a few measurements at 5 GeV, we use the more extensive 4 GeV data scaled down by a factor of 4, which reflects the approximate s^{-7} fall off of the cross sections. Since we are extrapolating from measured data, the estimates are likely good to about a factor of two.

The few hours needed to change kinematic settings are inconsequential compared to the entire experiment, and to the uncertainty in the time estimate, so we do not adjust the estimate by the time for the angle changes. Also, the kinematic coverage of the proton arm is such that the *ep* elastic scattering peak is within the acceptance, and the rates of *ep* elastic

scattering are small compared to the DAQ system capability of about 3 kHz. Thus, there is no need for additional calibration time for either the FPP or the calorimeter.

The electron beam has 80 % polarization and 30 μA current, and the photon flux is calculated for a 6 % radiator, with the incident beam energy at 5.5 GeV. If the beam energy is lower (higher), the photon flux will be somewhat reduced (increased). We note that the RCS experiment ran at 5.75 GeV with a 15 μA beam current, for the calorimeter at $\theta_{lab} = 20^\circ$ and a calorimeter distance from the target of 18 m. Our most forward angle setting, $\approx 17^\circ$, is close to the RCS setting mentioned above, but with twice the beam current, and about half the calorimeter distance, so the singles background rates are higher. The pedestal width (noise) was kept below 5 MeV for each of the RCS settings. This is more conservative than needed for the current experiment; We should be able to operate at the higher proposed luminosities of the current experiment with the widths below 20 MeV, so that the singles background rates in the calorimeter will not be a problem.

We plan to use a standard 15 cm (1.05 g/cm^2) liquid hydrogen target. With a spectrometer y-target acceptance of 10 cm, the end caps are always seen in the HRS, except for the $\cos\theta^{\pi}_{cm} = 0.6$ point, For a point target, the solid angle is about 6 msr; for the extended target, the solid angle averages to about 4 msr. The calorimeter distance to the target and the calorimeter thresholds that we will set lead to a capture fraction of 50 % – that is, half of the two-gamma neutral pion decays will be detected and accepted by the data acquisition system.

Previous experiments have demonstrated that systematic uncertainties on the polarization components are typically around 0.03 or so, so we set as a goal for the statistical uncertainties about 0.04 – 0.05. It is desirable to have similar size uncertainties for each of the points in the angular distribution. This is the case for $C_{x'}$, but spin transport in some kinematics increases the uncertainty of either p_y or $C_{z'}$ by factors of up to 3 – 4. Table V shows a run plan in which times have been slightly adjusted, leading to uncertainties on the favored spin component (and $C_{x'}$) that are slightly better than average, and the uncertainties on the unfavored component that are only slightly worse than average. Another consideration is that the GPD predictions are in the c.m. system, while we measure in the lab system. The spin rotation is not the same as the momentum rotation, so there is a spin precession between the frames. The precession angle is given in Table V. The precession gradually increases as we go to forward pion angles, at which the predicted polarization transfers are smaller, so there is no big difference in the angular distribution shapes in the two frames. At the smaller angles the two components are evenly mixed in going to the c.m. frame, so we do not need to further equalize the uncertainties at the forward pion angles. Except for the backward pion angle, the c.m. uncertainties for the two spin transfer components are in the range 0.05 – 0.08.

We expect that during the run we will "fine tune" the spectrometer central momentum setting at the largest pion angle, to further even out the uncertainties of the favored and unfavored spin components. The spectrometer central spin precession angle in this setting is 354° for the 4 GeV/c proton, leading to the increased uncertainty on $C_{z'}$. Simply shifting the momentum setting of the spectrometer down by 1 % should significantly reduce the uncertainty in $C_{z'}$, while keeping the ep elastic scattering within the acceptance.

COLLABORATION, CONFLICTING EXPERIMENTS, AND SCHEDULING

The core of the current collaboration consists of individuals who have been deeply involved in previous Hall A photon experiments, and who are FPP experts.

There are no conflicting experiments. While there are numerous meson photoproduction experiments that have been performed, or are awaiting beam time, at Jefferson Lab, none of these experiments attempts the high-energy measurements proposed here.

The experiment requires a "major installation", of the photon calorimeter, in Hall A. It would be beneficial if it were scheduled to run along with the RCS-II experiment, E03-003, which requires the same equipment and was approved for 7 days of beam time. The experiment does not require the development of any major new equipment. The two experiments will require a modified support structure base for BIGCAL, that corresponds to the 10 foot beamline height in Hall A, vs. the 13 foot height in Hall C. Such a change was already envisioned in the design of BIGCAL, as it is intended to be used in both Halls A and C.

[1] K. Wijesooriya *et al.*, Phys. Rev. C **66**, 034614 (2002).
[2] A. Afanasev, C. Carlson, and C. Wahlquist, Phys. Lett. B **398**, 292 (1997).
[3] G.R. Farrar, K. Huleihel, and H. Zhang, Nucl. Phys. B **349**, 655 (1991).
[4] R.A. Arndt, I.I. Strakovsky, and R.L. Workman, Phys. Rev. C **67**, 048201 (2003); R.A. Arndt, W.J. Briscoe, I.I. Strakovsky, and R.L. Workman, Phys. Rev. C **66**, 055213 (2002); see also `http://said.gwu.edu`.
[5] D. Drechsel *et al.*, Nucl. Phys. A **645**, 145 (1999); see also `http://maid.uni-mainz.de`.
[6] Hall A Experiment E99-114, C. Hyde-Wright, A. Nathan, and B. Wojtsekhowski, spokespeople. See `http://hallaweb.jlab.org/physics/experiments/RCS/public/`.
[7] C. Hadjidakis *et al.*, Phys. Lett. B **605**, 256 (2005); preprint hep-ex/0408005.
[8] H.W. Huang, R. Jakob, P. Kroll, K. Passek-Kumerički, Eur. Phys. J. C **33**, 91 (2004).
[9] L.Y. Zhu *et al.*, Phys. Rev. Lett. **91**, 022003 (2003).
[10] M. Diehl, Th. Feldmann, R. Jakob, and P. Kroll, Eur. Phys. J. C **39**, 1 (2005).
[11] D.J. Hamilton *et al.*, Phys. Rev. Lett. **94**, 242001 (2005); preprint nucl-ex/0410001.
[12] J. Ralston and B. Pire, Phys. Lett. B **117**, 233 (1982).
[13] M. Guidal, J.-M. Laget, and M. Vanderhaeghen, Nucl. Phys. A **627**, 645 (1997).
[14] D.S. Carman *et al.*, Phys. Rev. Lett. **90**, 131804 (2003).
[15] R. Shumacher and M. Mestayer, private communication.
[16] R. Gilman and A. Afanasev, unpublished.
[17] I.S. Barker, A. Donnachie, and J.K.Storrow, Nucl. Phys. B **95**, 347 (1975).
[18] W.-T. Chiang and F. Tabakin, Phys. Rev. C **55**, 2054 (1997).
[19] O. Gayou *et al.*, Phys. Rev. Lett. **88**, 092301 (2002).
[20] M.A. Shupe *et al.*, Phys. Rev. D **19**, 1921 (1979).